Helical Flows and Chaotic Mixing in Curved Micro Channels

F. Jiang, K. S. Drese, S. Hardt, M. Küpper, and F. Schönfeld
Institut für Mikrotechnik Mainz (IMM), Carl-Zeiss-Strasse 18-20, 55129 Mainz, Germany

DOI 10.1002/aic.10188

The mixing due to helical flows in curved micro channels is investigated. A new chaotic mixing mechanism is presented relying on alternately switching between different flow patterns exhibiting four Dean vortices. Flow patterns and interfacial stretching factors are numerically computed for various Dean numbers. For experimental studies a prototype of a chaotic mixer with curved channels was fabricated. The experimental evaluation of the mixing performance corroborates the numerical prediction: the mixing performance found for Dean numbers above 140 is qualitatively different from that at lower Dean numbers; the periodic switching between different vortex patterns leads to efficient mixing, manifesting itself in an exponential growth of interfacial area. In addition to the studies on mixing, residence-time distributions in the mixing channel are computed numerically. These investigations indicate that due to mass-transfer enhancement originating from the transversal redistribution of matter in the chaotic flow, hydrodynamic dispersion is substantially reduced relative to a straight channel. © 2004 American Institute of Chemical Engineers *AIChE J,* 50: 2297–2305, 2004
Keywords: microfluidics; micromixer; chaotic mixing; helical flows.

Introduction

Over the past decade, microfluidic devices have widely aroused interest for applications in bioanalytics or chemical process technology. In particular, the development of micromixers is a paramount task in the fields of μ-TAS, Lab-on-Chip systems and chemical microprocess technology. Contrary to macroscopic systems where turbulent flows are exploited, micromixing, governed by laminar flows, usually relies on diffusive mass transfer, which can be prohibitively slow when liquid-phase processes are considered.

Generally, the mechanisms which are employed for the enhancement of micromixing can be classified into two categories: active and passive measures. Although, active measures, such as internal stirring (Volpert et al., 2001), external variable-frequency pumping (Niu and Lee, 2003), and ultrasound agitation (Yang et al., 2001), can produce excellent mixing, they bring additional complications on system fabrication, and often need external energy sources. Several concepts, such as interdigital or split-and-recombine multilamination and chaotic mixing, have been proposed for passive micromixing (Ehrfeld et al., 1999; Schwesinger et al., 1996; Stroock et al., 2002). While the former approaches are generally applicable also for dispersive "mixing" of immiscible liquids, the latter approach of chaotic advection bears a high potential in the context of distributive mixing in confined geometries.

Various realizations of chaotic mixing in ducts of different geometries have been reported, among others, in the work of Jones et al. (1989) and Liu et al. (2000). Recently, in an alternative geometry, bas-relief microchannels, with so-called staggered herringbone structures at the walls, Stroock et al. (2002) reported that chaotic mixing had been achieved, and hydrodynamic dispersion was considerably reduced relative to that in a channel with unstructured walls.

A different concept of chaotic mixing was proposed by Schönfeld and Hardt (2003), and relies on helical flows induced in planar curved channels (Ghia and Sokhey, 1977;

Correspondence concerning this article should be addressed to F. Schönfeld at schoenfeld@imm-mainz.de.

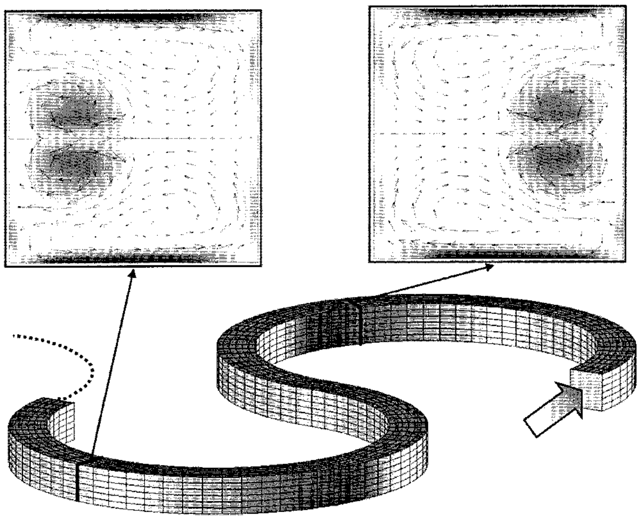

Figure 1. Meandering channel build up from two circular segments with corresponding secondary flow patterns (Schönfeld and Hardt, 2004).

(The arrow indicates the flow direction, the dashed line the continuation of the geometry).

Cheng et al., 1976). Here, in contrast to the designs reported previously, only a simple planar channel geometry without multistep or three-dimensional (3-D) structures is sufficient to induce chaotic mixing, as will be shown in the following paragraphs. To our knowledge this is the simplest channel architecture enabling chaotic mixing in the laminar regime.

The dimensionless groups characterizing such types of flow is the Reynolds number

$$\mathrm{Re} = u \cdot d/\nu \tag{1}$$

and the Dean number

$$K = \mathrm{Re}\sqrt{\frac{d}{R}} \tag{2}$$

Here, d denotes the hydraulic diameter, that is, four times the channel cross section divided by the perimeter, and R denotes the mean radius of curvature of the channel. A qualitative change in the secondary flow pattern is observed for Dean numbers above a critical value K_c of about 150. For $K > K_c$, the secondary flow consists of two counter-rotating vortices, whereas for $K < K_c$, two additional counter-rotating vortices appear close to the center of the outer channel wall (Cheng et al., 1976; Ghia and Sokhey, 1977).

The main idea about the mixing mechanism proposed in this article is based on the principle of chaotic advection by alternating superposition of different vortex patterns dating back to the work of Aref (1984). Aref showed that a chaotic flow may be induced when a liquid is stirred in such a way that a vortex periodically changes its location between two different positions. On this basis, Schönfeld and Hardt (2004) proposed a repeated switching between different four-vortex secondary flow patterns emerging in a curved channel, which can simply be achieved by changing the sign of curvature. This idea is illustrated in Figure 1.

The main objectives of the present study are the proof of proposed mixing concept, the numerical evaluation of the mixing performance, and its experimental validation.

On the basis of computational fluid dynamics (CFD) simulation results, a Lagrangian particle tracking technique was implemented, which allows the computation of interfacial stretching factors. As will be shown, the results clearly demonstrate that chaotic mixing occurs when the Dean number of the fluid flow is large enough.

In order to assess the influence of helical chaotic flows on hydrodynamic dispersion in this mixer, some calculations concerning the residence time distribution were also performed. The results indicate that hydrodynamic dispersion is expected to be restrained substantially relative to that of a straight channel.

In order to study mixing experimentally, a visualization method described earlier (Hessel et al., 2003) was used. The visualization is based on the formation of a colored compound from two transparent salt solutions. The local concentration of the colored compound is determined photometrically from the digitized images of the flow inside the channel. This method can provide information both on fluid layer formation at the very beginning, and during the course of mixing, as well as on the position where complete mixing has occurred. Experimental results verify that the mixing performance is deeply related to the structure of helical flow patterns formed inside the mixer.

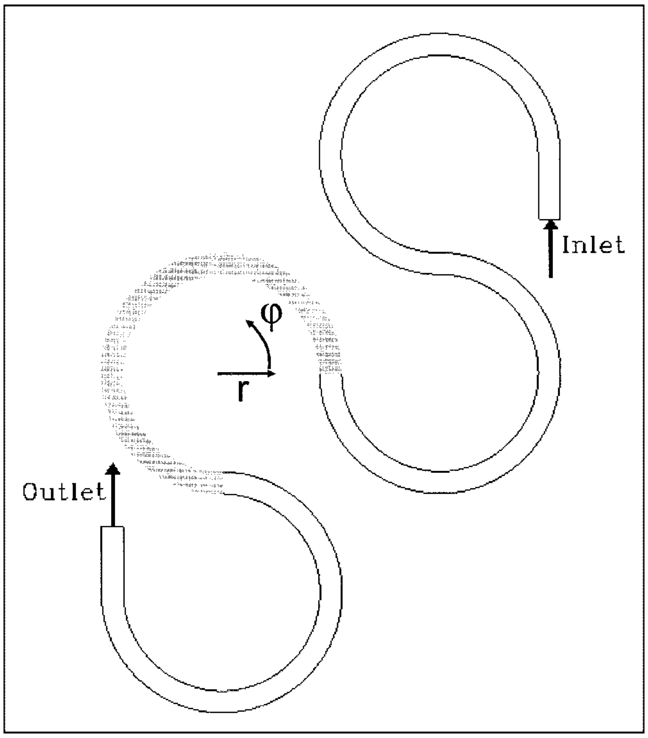

Figure 2. 4-element meander mixer.

The section shaded in gray denotes the base-element used for particle tracking. The z-direction is out of plane (not shown).

Model Geometry, Numerical Methods and Results

Motivated by the mixing concept outlined earlier, the flow field inside the mixing channel was computed numerically, especially in view of the helical flow patterns being formed. Exploiting the translational symmetry, a reduced model was used in the simulations. As shown in Figure 2, the model geometry consists of a channel comprising four circular arcs, and two straight inlet and outlet sections. Due to the periodicity of the geometry with respect to a translation by two circular elements, a periodic velocity field develops, with the exception of the region close to the inlet, where the flow is governed by entrance effects. Taking the periodicity in the geometry into account the flow field is completely characterized by the velocity field within a single circular-arc segment. In order to minimize entrance-flow effects, the region shaded in gray was chosen as the representative segment serving as the basis for studying the mixing efficiency. The lateral dimension d of the square channel was chosen to be 200 μm, and the radius of curvature R is 1,000 μm. A constant, uniform velocity and pressure was applied at the inlet and outlet, respectively. By inspection of the computed flow fields it was assured that a fully developed flow without any noticeable effect of the inlet and outlet boundaries was obtained in the third mixer segment for all Reynolds numbers under study.

The numerical computation of the mixing performance inside the meander mixer was performed via a two-step procedure. In the first step, the velocity and pressure fields were derived by solving the Navier-Stokes (N-S) equations, and the equation of mass conservation for an incompressible fluid, the physical properties of which were chosen to be those of water at temperature 25°C. In a second step, trajectories of massless particles were computed by streamline integration of the velocity field. Due to the aforementioned periodicity, and the symmetry (cf. Figure 1) of the flow field, arbitrarily long streamline integrations can be performed using the velocity field of a single element if entrance flow effects are neglected.

Flow computation

The velocity field was solved by using the commercial flow solver CFX4 (CFX/ANSYS), which is a multipurpose CFD software package, relying on the finite volume method (FVM). The SIMPLEC algorithm (van Doormal and Raithby, 1984) was used for pressure-velocity coupling, and the QUICK differencing scheme (Leonhard, 1979) for discretization of the velocity fields. For an accelerated convergence, the algebraic multigrid (AMG) iterative method was applied for solving the linearized algebraic equations. The reflection symmetry with respect to the r-ϕ plane (Figure 2) permits the simulation to be carried out only in half of the real geometry. A structured mesh with about 600,000 cells in total was used. The height and width of the half channel were resolved with 18 and 36 cells, respectively.

Particle tracking

The most straightforward way to quantify mixing properties is the solution of the advection-diffusion equation for a concentration field simultaneously to the solution of the N-S equation. However, especially for liquid/liquid mixing discretization errors, inducing artificial diffusive fluxes (numerical diffusion) are likely to dominate the simulation results on diffusive mixing (Fletcher 1997, Schönfeld and Hardt, 2004). In order to avoid such problems, Lagrangian particle tracking techniques, that is, the computation of trajectories of massless tracer particles, are commonly used to characterize mixing efficiencies (Aubin et al., 2003; Byrde and Sawley, 1999; Hobbs et al., 1997, 1998a,b,c; Hwang et al., 2002; Sawyers et al., 1996).

For particle tracking the flow velocity field is used as an input. In our studies, the velocity field was obtained from a CFD simulation, allowing the particle positions to be computed by time integration via

$$\vec{x}(t) = \int_0^t \vec{u}(\vec{x}(t'))dt' \tag{3}$$

with $\vec{n}$, $\vec{x}$ being the velocity and position vector, respectively. The integration was done for the representative channel segment of $3\pi/2$ arc length marked in Figure 2, using a second-order Runge-Kutta scheme with adaptive step-size control. This way, a Poincaré mapping is established, relating the particle positions at the outlet of the channel segment to the positions at its inlet. As the velocity field is periodic, iterated application of this Poincaré map allows computing the particle positions along the meander mixing channel over a large number of segments. The mapping and multistep integration of particle trajectories was performed using the commercial postprocessing software Fieldview9 (Intelligent Light). Initial positions of tracers were defined on the inlet patch of the corresponding channel segment, in the following referred to as element 1.

Two strategies of particle tracking were applied. First, for computation of interfacial stretching factors tracers were distributed along the "interface" of the two fluids (although not being a real interface as the fluids are miscible) on the inlet patch of element 1 (Sawyers, 1996). Assuming the inlet is fed by two merging fluids streams with the same flow rate, the projected interface is given by a straight vertical line in the center of the inlet patch. Subsequently, particle trajectories are computed by repeated integration as outlined earlier. After each integration step, the positions of all the tracers are recorded, and the length of the interface at the outlet patch is calculated by summing the distances between each pair of neighboring tracers. Since the amount of interfacial stretching is not uniform, the tracer density, that is, the distance between neighboring particles at the inlet, was locally readjusted according to the distance between adjacent tracers after integration, which was allowed to be 1 μm at maximum. In such a way, an iterative method for computing interfacial stretching is established. The iteration is terminated either if the final distance is smaller than 1 μm for each pair of neighboring tracers or if the total number of tracers exceeds 100,000.

As a second strategy, a large number of tracers were distributed uniformly over the whole inlet patch of element 1, each path of which was tracked through the flow field. The time at which the tracers penetrate the outlet patch of element 1 was recorded. When applying this procedure iteratively, the residence-time distribution inside the meandering mixing channel can be computed.

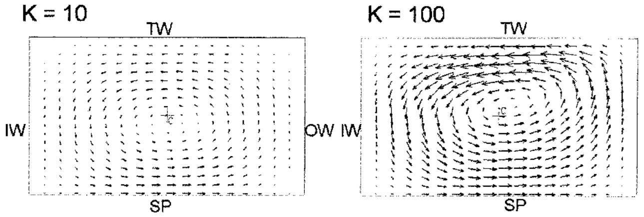

Figure 3. Helical flow pattern for Dean numbers of 10 and 100.

TW denotes the top wall, OW the outer wall, IW the inner wall, and SP symmetry plane of the r-z patch located at $\phi = \pi/2$. The velocity vectors are normalized with the corresponding volumetric flow rate.

Helical Flows

The mixing efficiency of the proposed meander mixer crucially depends on the secondary flow in the channel. Therefore, the characteristics of these inertially-induced flows are briefly discussed here. Typical flow patterns comprise two counter-rotating vortices above and below the symmetry plane (Dean, 1927, 1928), and the maximum in the velocity profile is shifted toward the outer channel wall. A qualitative change of the flow pattern occurs for Dean numbers above a critical Dean number K_c, which was determined to be about 140 for fully developed flow in curved square channels (Ghia and Sokhey, 1977). A slightly higher value of about 200 was derived in an earlier study (Cheng et al., 1976).

Figure 3 shows CFD results of the secondary flow in element 1 for Dean numbers of 10 and 100. The arrows represent a projection of the velocity vectors onto different z–r planes (cf. Figure 2), and only the upper half of the channel cross section is shown. The visualization plane was set at an angular position of $\phi = \pi/2$. For the smaller Dean number, the observed helical flow is weak, and the center of rotation is located close to the midpoint of the patch (C, denoted with a cross in Figure 3). When K rises to 100, the relative strength of the helical flow increases significantly, and the center of the vortex gets shifted toward the outer channel wall.

For a relatively high Dean number of 200, a significantly different flow pattern is found, as displayed in Figure 4. An additional counter-rotating vortex appears close to the outer channel wall. Figure 4 also indicates the evolution of the 4-vortex flow pattern along the mixing element, where ϕ varies from 0 to $3\pi/2$. Apparently the 4-vortex pattern is well developed already at $\phi = \pi/2$, even if at $\phi = 0$ a mirror-reflected pattern to $\phi = 3\pi/2$ is found. Such a symmetry is expected from the channel geometry and is exploited for the computation of particle trajectories, as outlined earlier.

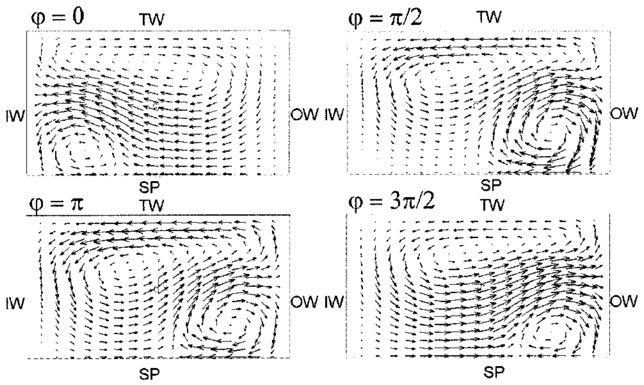

Figure 4. Evolution of the 4-vortex helical flow in a mixing element for K = 200.

The velocity vectors are normalized with the corresponding volumetric flow rate.

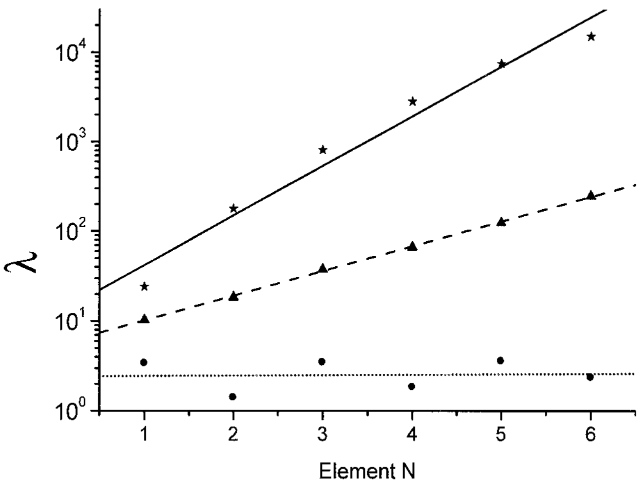

Figure 5. Interface stretching factor vs. element number for different Dean numbers (●: K = 10; ▲: K = 100; ★: K = 200).

Interface Stretching

Initially, the fluid interface is described by a vertical straight line across the inlet of the element 1. Due to the high interfacial stretching observed in some cases an iterative method was employed for interface tracking: evenly distributing 2,000 tracers over the inlet patch first, tracking their paths to some distance downstream, by repeatedly integrating over the velocity field of element 1, calculating the distance of each pair of neighboring tracers, using these distances to adjust the initial seeding density and then repeating the whole process until a satisfactory accuracy is achieved, or the total number of tracers exceeds 100,000. This seeding density adjustment can effectively eliminate interface self-crossing during particle tracking and improve the accuracy of interface stretching calculations.

The final tracer numbers for K = 10, 100, and 200 are about 3,000, 10,000 and 56,000, respectively. The derived interface stretching factors are plotted in Figure 5 as a function of the number of mixing segments the flow has traversed. The interface stretching factor λ is defined as the interface length at a certain position divided by the initial interface length. From the figure, it is obvious that at K = 10 nearly no stretching occurs, while for K = 100 and 200, the data points are better compatible with an exponential growth of the form

$$\lambda = Me^{\mu N} \tag{4}$$

where N denotes the number of the mixing element. The parameters of the fit functions are given as $M = 5.403$, $\mu = 0.633$ (K = 100), and $M = 11.733$, $\mu = 1.274$ (K = 200), respectively. The exponential factor μ can be related to a positive Lyapunov exponent Λ by $\mu = \Lambda/c$ (Sawyers et al., 1996), with c being a constant relevant to model geometry. The exponential growth of the interface and the positive Lyapunov exponent indicate the occurrence of chaotic mixing at large Dean numbers. However, the mechanism by which chaotic advection is induced is different for $K = 100$ and $K = 200$. In the former case the chaotic flow can be described by the scenario first outlined by Aref (Aref 1984). Since the center of rotation of the two Dean vortices changes with changing sign of curvature (cf. Figure 3), the meandering channel induces vortices with alternating positions. For $K = 200$, four vortices are present, and the flow pattern shows a pronounced asymmetry. Thus, the change of the sign of curvature causes a drastic change in the flow pattern. These repetitive changes induce a strong chaotic flow.

For $K = 10$, the vortices are comparatively weak and are approximately symmetric with respect to the ϕ-z symmetry surfaces of the channel segments. Because of that reflection symmetry, the inversion of the channel curvature in the following mixing element more or less only inverts the rotation direction of the vortex. It is, thus, expected that after two-mixing elements, the interface is approximately brought back to its original position. This process is successively repeated in mixing elements further downstream, and mixing should be very slow. For $K = 100$, the helical flow is stronger than for $K = 10$ (cf. Figure 3). In addition to that, the vortex centers are shifted toward the outer channel wall, and the reflection symmetry described above is broken. Hence, the vortices occurring in two successive mixing elements are centered around different positions on the channel cross-sectional plane. This way a "blinking-vortex" flow pattern similar as described by Aref (1984) is created, and chaotic mixing is induced. For $K = 200$, two additional counter- rotating vortices close to the outer channel wall appear (cf. Figure 4). The vortex patterns superposed in successive mixing elements are now substantially different, leading to a further enhancement of chaotic mixing. As suggested by the data points in Figure 5, there may be some deviations from an exponential increase of interfacial area in this case. A possible explanation for this observation is errors in the computation of the interfacial length when the stretching is very large. Most likely, the length of an extremely stretched and folded interface is underestimated by adding distances between neighboring tracer points.

Ghia and Sokhey's (1977) results indicate that in curved channels the change of helical flow pattern from two to four vortices happens at $K = 143$. Our simulation results (not shown here) testify that when $K = 150$, this change has already happened.

Shapes of interfaces in the upper half of the cross-sectional planes are shown in Figure 6. For the sake of brevity, only the results for the first two-mixing elements are shown for $K = 10$ and $K = 100$. These diagrams corroborate the discussion of the previous paragraphs. For $K = 200$, the interface after the 6th mixing element is additionally included, indicating the high degree of interfacial stretching.

In order to assess the accuracy of the derived numerical results, two types of tests were performed. In the first one, the dependence of the interface stretching factors on the grid resolution of the CFD calculations was studied. For this purpose, a Richardson extrapolation for the stretching factors as a function of 1/(number of grid cells) was computed, based on numerical grids with 30,000, 180,000, and 600,000 cells. As a result, the value based on 600,000 cells only deviates by 2% from the extrapolated value for a Dean number of 200 (which is the most critical among the scenarios studied in this work).

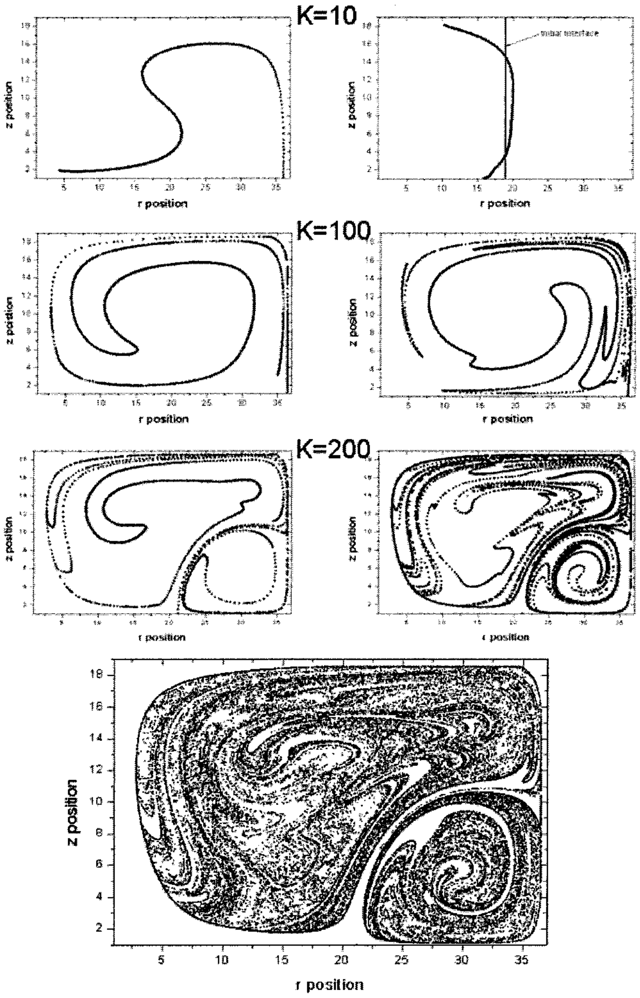

Figure 6. Interface shapes obtained from particle tracking for K = 10 (upper row), K = 100 (middle row), and K = 200 (lower row).

The left column shows the shapes after the first mixing element;the right column shows those after the second mixing element. The initial interface position is indicated in the diagram in the upper right corner. The r, z positions are scaled with corresponding differentiated cell dimensions.

In the second test, the dependence of the stretching factors on the number of particles tracked was studied. In this context the final particle number obtained from the iterative seeding process was used. Now, a Richardson extrapolation as a function of 1/(number of tracer particles) was computed, based on particle numbers of 19,000, 44,000, and 56,000 for $K = 200$. The results obtained with the highest seeding density agree within a 10% error with the extrapolated value when three mixing elements are considered. For the sixth mixing elements, the error increases to 17%. The longer the tracking distance, the more severe are the numerical errors. As already indicated above, when the interface gets deformed very heavily, the algorithm for computing the interfacial length becomes inaccurate, hence, possibly underestimating the corresponding line

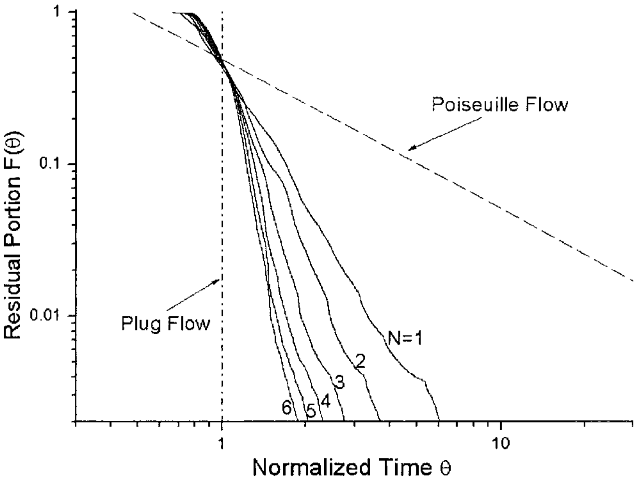

Figure 7. Residual portion of particles remaining in the meander mixer for $K = 200$.

integral. The Richardson extrapolation supports the hypothesis that for large Dean numbers the stretching factors are underestimated. For lower Dean numbers, that is, $K = 10$ and 100, the deviations are much smaller, less than 5% for all six mixing elements examined, although the final tracer numbers are smaller.

Residence Time Distribution (RTD)

The RTD for fluids in the meander mixer was calculated by tracking ~80,000 uniformly distributed tracers initially seeded over the inlet patch of the "first" mixing element, covering the whole cross section. Each particle trajectory was tracked through the flow via integration of Eq. 2. Whenever a particle reached an outlet of a mixing element, the residence time τ was recorded. The τ values of all the tracers with respect to a same downstream outlet allow computing the RTD of tracers with zero diffusivity. For a given time t, the number of tracers $N(t)$ with a residence time τ less than t was calculated; if the total number of tracers is denoted with N_{tot}, the residual portion of particles remaining in the mixer is given as

$$F(t) = 1.0 - \frac{N(t)}{N_{tot}} \tag{5}$$

which was used to evaluate the RTD in this article. Additionally, the actual residence time τ was normalized by the residence time of an assumed particle traveling at the average flow velocity to obtain the normalized RTD $F(\theta)$, with θ being the dimensionless time.

The RTDs for $K = 200$ after mixing element 1 to 6 are plotted in Figure 7, along with the RTDs for Poiseuille and for plug flow in a straight square channel with the same cross-sectional dimension. The RTDs in the meander mixer asymptotically approach those of plug flow, and are much narrower than those of Poiseuille flow. With the fluid flow proceeding further downstream, the RTD in the meander mixer becomes increasingly better. This is a result of the chaotic flow forming in the mixer which homogenize the flow and may be used to restrain hydrodynamic dispersions in practice.

By averaging the residence times of all the tracers with exclusion of 2% of the tracers which are very close to the channel walls, the residence time derived from the average volumetric flow rate can be recovered with a deviation less than 1%. In Figure 7 the curve relevant to Poiseuille flow was derived from the analytical Poiseuille velocity profile of fluid flow in a comparable straight square channel. In order to further check the reliability of the numerical results, the RTD for a straight channel was also computed based on a CFD using the same methods and mesh density as for the meander mixer. Simulation and analytical results coincide perfectly, for this reason the simulated curve for Poiseuille flow was not included Figure 7.

Experimental Methods and Results

A scaled-up version of the meander mixer structure schematically described in Figure 2 was realized in polymethylmethacrylate (PMMA). The channel was micromachined by precision milling having a 1 mm^2 cross-section, and a length of 322 mm, corresponding to 20 mixing elements. Sealing of the channel was done by a 100 μm PMMA-foil attached by solvent bonding. Transparent plastic tubing of about 1.4 mm inner diameter was connected to the two inlets and the outlet via 1/8 in. steel tube connectors. Two continuously working double-action syringe pumps (Desaga mod. KP 2000, Germany, 10 mL piston volume each) were used for liquid pumping. The pulsations of the step motors were damped by a 20 mL gas ballast. Detection of color changes due to the chemical reaction used for visualization of mixing, as well as documentation of flow patterns was done using digital video equipment (Sony DXC-930 P color video camera, PC with digitizer-card) with planar illumination from a fluorescence light source from below. Overall flow-rates ranged from 200–2,000 mL h^{-1} adjusted by the double-action syringe pumps. Accuracy measurements of the mass-flow affirmed an error of about 0.3% at worst in the flow-range considered. The corresponding Dean numbers

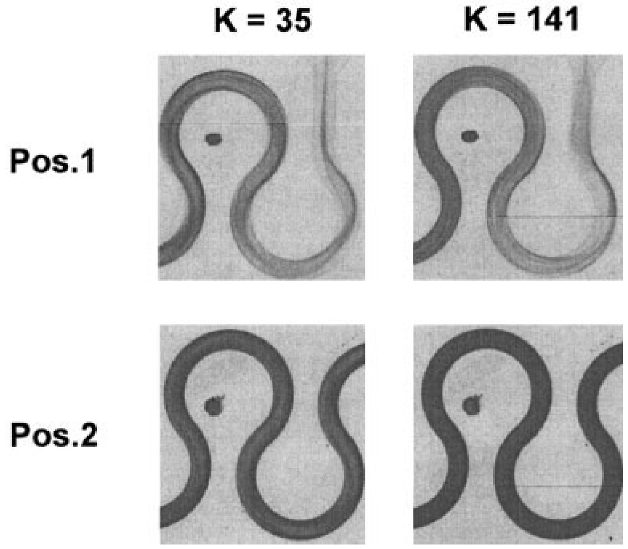

Figure 8. Microphotographs of the mixing patterns in the meander mixer for different Dean numbers and positions.

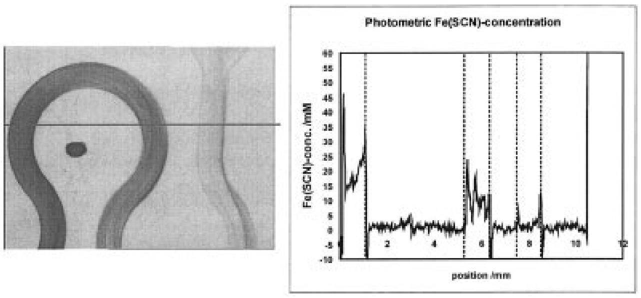

Figure 9. Left: Microphotograph of the flow patterns obtained from the mixing and reaction of a 50 mM $Fe(NO_3)_3$ solution with a 50 mM NaSCN solution for K = 246, taken close to the inlet of the mixer (the horizontal line denotes the cut over which the concentration was determined); right: resulting photometric concentration profile.

The dashed lines enclose the channel regions.

tested ranged from 35 to 351. Mixing visualization was realized by employing a very fast ionic dye reaction (Hessel et al., 2003), that is, aqueous solutions of Iron(III)-nitrate and Sodium-rhodanide, forming the intensely reddish Fe(III)-rhodanide after a 1:1-stoichiometric reaction.

In a first experiment, different points along the channel were marked by dots in order to re-address positions for qualitatively comparing the flow-patterns at the respective location along the channel. In Figure 8 microphotographs for $K = 35$ and 141 are presented to show the structure of the flow patterns observed. Flow patterns from the mixing and reaction of a 50 mM $Fe(NO_3)_3$ solution with 50 mM NaSCN solution at 25°C were recorded for the inlet section (Pos. 1), showing the first and the second mixing element, and at a position 118 mm downstream (Pos. 2), showing mixing elements No. 7 and 8.

It can be seen that even if the residence time for the $K = 141$ flow is about a factor of 4 smaller than for the $K = 35$ at the same position, mixing has proceeded to a higher degree for the larger Dean number, as clearly visible especially when comparing the images recorded at Pos. 2.

A quantitative evaluation of the mixing performance is done photometrically by determining the local concentration of the colored solution from the digitized images. According to the Lambert-Beer law, the local concentration c can be measured by photometry via the relation

$$\ln \frac{\Phi_0}{\Phi} = \varepsilon c l \tag{6}$$

where Φ (Φ_0) denotes the photometric brightness obtained from the digitized images with finite (zero) rhodanite concentration, ε is the extinction coefficient, c is the $Fe(SCN)_3$ concentration in the dyed solution, and l is the layer thickness. With a maximum extinction of 150 equaling 50 Mm, and a minimum extinction of 234 equaling 0 mM, the extinction coefficient ε is accessible. From this, concentration values averaged over the height of the channel can be determined.

The image on the left of Figure 9 shows a microphotograph of the mixing patterns obtained for a reaction of a 50 mM $Fe(NO_3)_3$ solution with 50 mM NaSCN solution at 25°C and K = 246 close to the inlet of the mixer. The diagram on the right shows the associated photometric concentration profile over a cut appearing as a horizontal line on the left. At first, only one lamella is visible representing about 10 mM of reaction product. The next profile recorded further downstream already shows a multitude of lamellae representing between 2 and 24 mM of product. With mixing advancing, the flow pattern shows fewer and fewer lamellae, and increased product content between 15 and 28 mM.

The image on the left side of Figure 10 illustrates the mixing patterns obtained from the reaction of a 50 mM $Fe(NO_3)_3$ solution with 50 mM NaSCN solution in the region of near-complete mixing. Over the first cross-section on the righthand side of Figure 10, the concentration profile still exhibits some variations. When going further downstream (concentration peak in the middle and on the left), these variations get leveled out, and the concentration increases to values close to 50 mM which indicates complete mixing. In the concentration profile of Figure 10 spikes of concentration values above 50 mM and below 0 occur. These are artifacts originating from the illumination which is not completely perpendicular from below but partly tilted. Thus, values above 50 mM derive from shadows, and those below 0 from illuminated channel walls. From the base-line noise of the concentration profiles the uncertainty can be read off to be about ±2 mM.

As stated earlier, a product concentration of 50 mM designates the position of complete mixing, which allows us to calculate the mixing time t_m via

$$t_m = \frac{l_m A}{\dot{V}} \tag{7}$$

where t_m denotes the time until complete mixing, l_m distance from the inlet to the position of complete mixing, A the channel cross-section and $\dot{V}$ the volumetric flow rate.

The dependence of mixing time on the Dean number is shown in Figure 11. The lower limit of the x-axis in this diagram is determined by the minimum volume flow for which

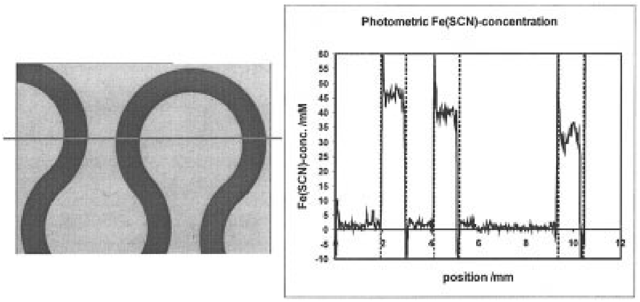

Figure 10. Left: Microphotograph of the flow patterns obtained from the mixing and reaction of a 50 mM $Fe(NO_3)_3$ solution with a 50 mM NaSCN solution for K = 246, taken in the region of near-complete mixing (the horizontal line denotes the cut over which the concentration was determined); right: resulting photometric concentration profile.

The dashed lines enclose the channel regions.

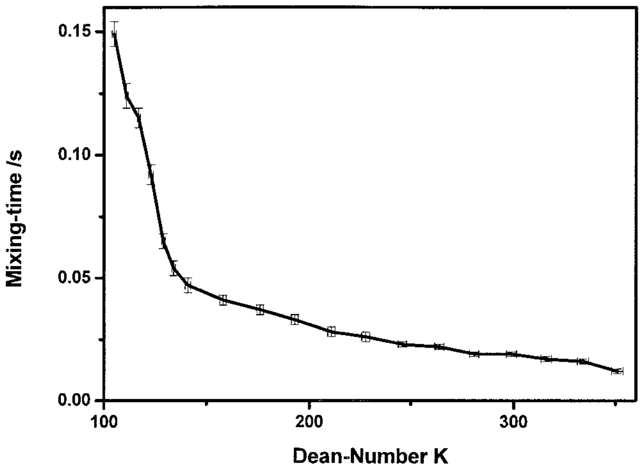

Figure 11. Mixing-time vs. Dean-number in the meander mixer.

The line connecting the data points should guide the eye.

mixing is completed within the meandering channel. Clearly, a strong reduction of the mixing time is observable in the range between $K = 105$ and 141. At $K = 141$, the mixing behavior changes. From then on, only a comparatively slow, but steady, reduction results from a further increase of the Dean number. The preceding simulation results indicate that, when the Dean number increases over 140–150, the helical flow pattern switches from the two to the four vortex version. This is in good accordance with an independent numerical analysis from which a change was calculated to occur at $K = 143$. (Ghia and Sokhey, 1977). From the experiments, there is clear evidence for a drastic change of the flow pattern for Dean numbers around 140. It should be noted that variations of the mixing time can only be due to a change of the flow pattern inside the mixer. For Dean numbers smaller than 140, the relative strength of the helical flow (as compared to the mean flow velocity) increases with K. In addition to that, the centers of the vortices are more and more shifted toward the outer channel wall. Due to this phenomenon, the "blinking vortex" principle for inducing chaos becomes more and more effective. For Dean numbers above the critical value related to the four-vortex pattern, a further increase of K still reduces the mixing time, but not as rapidly as in the case of subcritical Dean numbers. Obviously, in this regime the flow pattern is comparatively stable with respect to a further increase of the Dean number.

In order to estimate the accuracy of the obtained experimental results, an error propagation analysis was performed. Assuming the mixing length l_m, the channel width d, the radius of curvature R, and the volumetric flow rate $\dot{V}$ as independent variables, the dependence of the Dean number $K = K(d,R,\dot{V})$, and the mixing time $t_m = t_m(l_m,d,\dot{V})$ on these parameters was analyzed using the error-propagation formula

$$Err = \sum_{i=1}^{N} \frac{\partial f}{\partial x_i} dx_i \tag{8}$$

where f is either K or t_m and x_i are the independent variables. From the manufacturing process for the meander mixer, inaccuracies of the geometric parameters d and R are in the range of ± 10 μm. Together with the volume-flow inaccuracies, this leads to a relative error in the Dean number of 2% at $K = 35$, and of about 1% at $K = 351$. The strongest influence for the determination of mixing time comes from the error in determining l_m, which is assumed to be ± 5 mm. In total, an error in t_m of about 4% at $K = 35$, and 8% at $K = 351$ is found. The corresponding uncertainties are plotted as error bars in Figure 11.

Summary and Conclusions

The key to realize chaotic mixing in microfluidic devices is to activate strong enough transverse flow components, and to superpose these secondary flows in the manner of "blinking vortices". On the basis of this principle, a meander mixer was designed consisting of a series of channel segments of alternating curvature. The evolution of helical flows and fluid interfaces in such channels was studied using CFD methods together with streamline tracking techniques. These simulations indicate that for low Dean numbers (≈ 10), no chaotic mixing occurs, rather than that the interface approximately moves back to its original position when the channel curvature is reversed. Already at Dean numbers around 100, the interface length increases exponentially in downstream direction. This exponential interface stretching even gets enhanced when two additional counter-rotating vortices appear in the channel, which is the case for Dean numbers larger than 143. Exponential interface stretching can be translated to a positive Lyapunov exponent, indicating that in this regime chaotic mixing occurs.

In addition to the studies on mixing, the residence-time distribution of tracers with zero diffusivity was computed using methods of particle tracking. The chaotic transversal flows were found to have a favorable impact on the RTD, coming close to a plug-flow regime after the fluid has passed through a couple of mixing elements.

Parallel to the simulations, experiments were conducted in order to study the mixing performance of the meander mixer. For characterization of mixing, two transparent salt solutions were used forming a colored compound when the corresponding ionic species get in contact. The local concentration of this compound was determined photometrically from the digitized images of the flow patterns inside the channels. This technique allows determining the position of complete mixing and, derived from that, the mixing time. A distinct change in the mixing performance was found at a Dean number of about 140, in accordance with the predicted transition of the secondary flow pattern. In this regime, mixing times below 50 ms are reached. For the geometry chosen, a Dean number of 140 corresponds to a Reynolds number of about 313, almost an order of magnitude smaller than the critical Reynolds number for the laminar-to-turbulent transition in a straight channel. Hence, the proposed meander mixer offers an efficient means for fast mixing in a regime where mass transfer is usually slow and dominated by diffusion. In order to utilize the full potential of the mixer it should be operated at $K > 140$. In contrast to designs proposed by other authors, it is easy to fabricate, does not require sophisticated microstructures, and can be realized in a planar geometry. It is, therefore, conceivable so that it will find widespread applications in various areas of microfluidics.

Acknowledgment

The work has been partly supported by the DFG-Forschergruppe FOR 516/1 and by the German Ministry of Research and Education, grant number 16SV1355.

Literature Cited

Aref, H., "Stirring by Chaotic Advection," *J. Fluid Mech.*, **143**, 1 (1984).

Aubin, J., D. F. Fletcher, and C. Xuereb, "Characterization of Mixing Quality in Micromixers," *Chem. Eng. and Technol.,* **26**(12), 1262 (2003).

Byrde, O., and M. L. Sawley, "Optimization of a Kenics Static Mixer for Non-Creeping Flow Conditions," *Chem. Eng. J.*, **72**, 163 (1999).

Cheng, K. C., R. C. Lin, and J. W. Ou, "Fully Developed Laminar Flow in Curved Ducts of Rectangular Channels," Trans. of ASME: *J. of Fluids Eng.*, 41 (1976).

Ehrfeld, W., K. Golbig, V. Hessel, H. Löwe, and T. Richter, "Characterization of Mixing in Micromixers by a Test Reaction: Single Mixing Units and Mixer Arrays," *Ind. Eng. Chem. Res.*, **38**, 1075 (1999).

Fletcher, C. A. J., *Computational Techniques for Fluid Dynamics*, 2nd ed., Springer, Berlin (1997).

Ghia, K. N., and J. S. Sokhey, "Laminar Incompressible Viscous Flow in Curved Ducts of Regular Cross-Sections," Trans. of ASME: *J. of Fluids Eng.*, 640 (1977).

Hessel, V., S. Hardt, H. Löwe, and F. Schönfeld, "Laminar Mixing in Different Interdigital Micromixers: I. Experimental Characterization," *AIChE J.*, **49**, 566 (2003).

Hobbs, D. M., and F. J. Muzzio, "The Kenics Static Mixer: a Three-Dimensional Chaotic Flow," *Chem. Eng. J.*, **67**, 153 (1997).

Hobbs, D. M., and F. J. Muzzio, "Optimization of a Static Mixer Using Dynamical Systems Techniques," *Chem. Eng. Sci.*, **53**, 3199 (1998[a]).

Hobbs, D. M., and F. J. Muzzio, "Reynolds Number Effects on Laminar Mixing in the Kenics Static Mixer," *Chem. Eng. J.*, **70**, 93 (1998[b]).

Hobbs, D. M., P. D. Swanson, and F. J. Muzzio, "Numerical Characterization of Low Reynolds Number Flow in the Kenics Static Mixer," *Chem. Eng. Sci.*, **53**, 1565 (1998[c]).

Hwang, W. R., H. S. Jun, and T. H. Kwon, "Experiments on Chaotic Mixing in a Screw Channel Flow," *AIChE J.*, **48**, 8 (2002).

Jones, S. W., O. M. Thomas, and H. Aref, "Chaotic Advection by Laminar Flow in a Twisted Pipe,"*J. Fluid Mech.*, **209**, 335 (1989).

Leonard, B.P., "A stable and Accurate Convection Modelling Procedure Based on Quadratic Upstream Interpolation," *Comput. Meth. Appl. Mech. Eng.,* **19**, 59 (1979).

Liu, R. H., M. A. Stremler, K. V. Sharp, M. G. Olsen, J. G. Santiago, R. J. Adrian, H. Aref, and D. J. Beebe, "Passive Mixing in a Three-Dimensional Serpentine Microchannel,"*J. of Microelectromechanical Systems*, **9**, 190 (2000).

Niu, X., and Y. Lee, "Efficient Spatial-Temporal Chaotic Mixing in Microchannels," *J. Micromech. Microeng.*, **13**, 454 (2003).

Sawyers, D. R., M. Sen, and H. C. Chang, "Effect of Chaotic Interfacial Stretching on Bimolecular Chemical Reaction in Helical-coil Reactors," *Chem. Eng. J.*, **64**, 129 (1996).

Schönfeld, F., and S. Hardt, "Simulation of Helical Flows in Micro Channels," *AIChE J.,***50**, 771 (April 2004).

Schwesinger, N., T. Frank, and H. Wurmus, "A Modular Microfluidic System with an Integrated Micromixer,"*J. Micromech. Microeng*, **6**, 99 (1996).

Stroock, A. D., S. K. W. Dertinger, A. Ajdari, I. Mezic, H. A. Stone, and G. M. Whitesides, "Chaotic Mixer for Microchannels,"*Science*, **295**, 647 (2002).

Van Doormal, J. P., and G. D. Raithby, "Enhancement of the SIMPLE Method for Predicting Incompressible Fluid Flows," *Numerical Heat Transf.*, **7**, 147 (1984).

Volpert, M., I. Mezic, C. D. Meinhart, and M. Dahleh, "Modeling and Numerical Analysis of Mixing in an Actively Controlled Micromixer," *Proc. of the First Int. Conf. on Heat Transfer, Fluid Mechanics and Thermophysics*, Kruger Park, South Africa 2002).

Yang, Z., S. Matsumoto, H. Goto, M. Matsumoto, and R. Maeda, "Ultrasonic Micromixer for Microfluidic Systems," *Sensors and Actuators*, **A93**, 266 (2001).

Manuscript received Nov. 21, 2003, and revision received Jan. 15, 2004.